Development of a small-scale actuator disk

Author
SANNE DE JONG HELVIG

Supervisor
R. JASON HEARST

December 17, 2019

NTNU – Trondheim
Norwegian University of
Science and Technology

Table of Contents

Figures

List of Acronyms

ABL Atmospheric Boundary Layer. 5

AD Actuaor Disk. 4, 6–9, 11–13, 15, 16, 18, 21, 22, 24, 25

CFD Computational Fluid Dynamics. 7, 11

NUD Non-Uniform Disk. 13, 14, 22, 24

PIV Particle Image Velocimetry. 9–11, 25

RWTM Rotating Wind Turbine Model. 6, 9, 12, 15, 16, 18–20, 22, 25

UHD Uniform Holes Disk. 13, 14, 22, 24

WGTM Wake-Generating Turbine Model. 6, 10, 14–16

Abstract

The drag of a small-scale rotating wind turbine model was measured in a wind tunnel, and compared to the drag of different actuator disks, in order to find the actuator disk that most resembles the rotating model. The actuator disks were created with two different designs, one with uniform holes and one non-uniform, and three different solidities were used for each design. A solid disk was also tested as a reference. The drag on the actuator disks was measured in the wind tunnel in the same manner as with the rotating model, using five different Reynolds numbers. When conducting the experiments, several measurements of the rotating models had to be conducted due to deviations in the measurement data. Some of these deviations were regarded as outliers and discarded, and the average was taken of the remaining measurements. This resulted in a drag coefficient profile which was compared to the drag coefficient profiles representing the different actuator disks. The disk with a non-uniform design and a solidity of 35% turned out to be the closest match, while the disk with uniform holes and a solidity of 35% was the second closest match. Assuming a Gaussian distribution of the drag coefficients, both of the disks with 35% solidity overlap with the rotating model's drag coefficient within their standard deviations, showing that it is reasonable to use these actuator disks in place of a rotating model.

Oppsummering

Motstandskraften til en småskala roterende vindturbinmodell ble målt i en vindtunell, og sammenlignet med motstandskraften til ulike aktuatordisker, for å finne den aktuatordisken som ligner mest på den roterende modellen. Aktuatordiskene ble laget med to ulike design, en med uniforme hull og en ikke-uniform, og tre ulike tettheter ble brukt for hvert design. En solid disk ble også testet som en referanse. Motstandskraften til aktuatordiskene ble målt i vindtunellen på samme måte som for de roterende modellene, ved å bruke fem ulike Reynoldstall. Flere målinger av de roterende modellene ble gjennomført på grunn av avvik i måledataene. Noen av disse avvikene ble ansett som uteliggere og forkastet, før gjennomsnittet av de gjenværende målingene ble funnet. Dette resulterte i en dragkoeffisientprofil som ble sammenlignet med dragkoeffisientprofilene til de ulike aktuatordiskene. Disken med et ikke-uniformt design og 35% tetthet viste seg å samstemme best, etterfulgt av disken med uniforme hull og 35% tetthet. Hvis man antar at dragkoeffisientene er normalfordelte, overlapper begge diskene med 35% tetthet med den roterende modellen sin dragkoeffisient innenfor sine standardavvik, noe som viser at det er rimelig å bruke disse aktuatordiskene i stedet for en roterende modell.

Acknowledgements

I would first and foremost like to thank my supervisor Jason Hearst, for always helping me out and supporting me, and for sparking my interest in aerodynamics in the first place. Through weekly meetings he has continued to push me and give me helpful input every step of the way, and he was always available when I needed guidance.

Secondly, I would like to thank Magnus Kyrkjebø Vinnes, for helping me out whenever I got stuck and for his patience and positivity whenever we were troubleshooting. My thesis would not be what it is without your guidance.

I also want to thank Lars Morten Bardal, for teaching me how to do calibrations, how to use the wind tunnel and for making the LabView program that he so kindly let me use.

Further, I want to give my thanks to Olav Rømcke for teaching me how to use power tools, and the rest of Jason's Ph.D. students for all their helpful input at our weekly meetings.

Finally, I want to thank Adrian Bogen Skibelid, for proof reading, for all our sessions of throwing ideas back and forth, and for your continuous support.

Chapter 1

Introduction

In a world with an expanding population, growing standards of living [1], and with it, an increasing need for energy, simultaneous with a spreading focus on sustainability and environmentally friendly solutions [2, 3], renewable energy has never been more relevant. The amount of onshore and offshore wind power is increasing [4], and numerous companies are working to find their role in the new market. Optimizing wind turbines and wind farms is an important aim, and researchers are using both simulations and experimental methods in order to explore different potentially efficient solutions.

However, both when doing experiments and simulations, modeling a wind farm with moving blades is often extremely complicated. Thus, simplifications, such as the Actuaor Disk (AD), are commonly adopted. The idea of the AD is that it produces the same drag as the wind turbine, resulting in similar bulk characteristics in the wake. The physical wind tunnel analogue to an AD is a static, porous disk. However, at this point in time, there are no clear directions and no scientific consensus on how to design and make these porous disks in order to mimic rotating turbines when conducting experiments.

1.1 Problem formulation

The objective of the project described in this thesis is to develop a static, porous disk that has approximately matched characteristics to a small rotating wind turbine model provided by KTH, by matching the produced drag.

Chapter 2

Background

Renewable energy now accounts for a third of global power capacity [5], and according to Siemens, wind power alone may represent one third of the global electric demand by 2040 [6]. However, to realize these types of targets, larger wind farms covering increasingly larger surface areas are required [7, 8]. Placing the turbines in wind farms is the most economic and efficient in terms of planning, maintenance, and use of land and infrastructure [9]. However, this means that the turbines are permanently exposed to the turbulent wakes caused by upstream rows of turbines [10]. Additionally, current utility-scale turbines extend a significant distance into the Atmospheric Boundary Layer (ABL), which is naturally turbulent [9, 10].

The wake stemming from upstream wind turbines determines how much power a downstream turbine can generate and what mechanical load it experiences, meaning that the study and characterization of wind turbine wakes has become an important research area [9, 10]. According to a review paper by Veers et al. [3], the first grand challenge in wind energy research today is to improve the understanding of wind power plant flow physics. According to another review by Porté-Agel et al. [11], there is a need for further developing models for wind farm wake flows and investigating the role of atmospheric turbulence, as well as to extend wind farm studies to include factors such as topography and thermal stability.

Variability in the power output due to unsteady characteristics of the ABL is another challenge for the integration of large amounts of wind energy into the electricity grid. The need for fill-in power and stronger components made to withstand unsteady loads turns the problem into that of a cost-minimizing problem, in order for wind energy to achieve the desired market share [12].

Studies of the interaction of large wind farms and the ABL are currently not prevalent. Neither are studies on how the wake develops and interacts with downstream wind turbine arrays. Deeper understanding of these phenomena is required in order for wind farm

developers to plan better-performing, less maintenance-intensive and longer-lasting wind farms, and for manufacturers to create better fatigue load-mitigating designs [10, 13].

Field tests are being carried out, but such approaches are expensive, difficult and by their nature incapable of being completely controlled [14]. Even though there is a need for more data from actual wind farms to evaluate experimental results, wind tunnel experiments have the advantage that the boundary conditions can be carefully controlled [12]. A challenge when studying wind farms in wind tunnels is performing measurements with sufficiently high spatial resolution, which has made small-scale turbines relevant, combined with the reduced costs related to smaller models [15]. The experts workshop organized by ForWind-Uni Oldenburg in 2018 on Wind Energy Science & Wind Tunnel Experiments agreed to qualify the smallest wind turbine models, with a rotor diameter less than 0.5 m, as Wake-Generating Turbine Model (WGTM) [13].

However, using rotating blades for such small rotors, and building and operating more than a hundred of them, is not practical, but rather complex and costly. In addition, scaled rotating wind turbine models have limitations since perfect flow similarity is not possible due to large scale differences [12]. Thus, it is often convenient to use simplifications, a common one being the AD concept. The physical representation of an AD is a static, porous disk, with a solidity defined as the ratio between the area that is solid and the total area of the disk. Such porous disks work as drag sources and do not directly extract energy from the flow, in contrast to actual wind turbines, but instead dissipate the kinetic energy of the incoming wind by generating small-scale turbulence in the near wake of the disk [16].

2.1 Actuator disk research

Many researcher have looked into ADs, most studying the disk itself and comparing it to rotating models [9, 13, 14, 17, 18, 19, 20, 21], however some have gone so far as to use ADs to model wind farms [12, 22, 23].

The first requirement for a simplified wind turbine model is correct characterization of the wake [22]. When creating an AD, the starting point is often to match the diameter and the drag coefficient, defined as

$$C_D = \frac{D}{\frac{1}{2}\rho U^2 A} \tag{2.1}$$

where ρ is density, U is the mean flow velocity and A is the reference area, typically $A = \pi r^2$. Studies have shown that the drag coefficient is only weakly dependent on Reynolds number [18].

When comparing ADs and Rotating Wind Turbine Models (RWTMs), studies conducted so far are in general agreement on the following terms. The near wake differs between the two models, as the rotating turbines introduce rotational momentum, tip and hub vortices, and turbulence from the blades, while the turbulence in terms of the AD is produced

by porous blockage [17, 24, 25]. The difference in flow behavior in the near wake, especially prominent in terms of velocity deficit and turbulence intensity, is thus caused by fundamentally different turbulence production and mixing mechanisms [13, 16, 26].

However, blade signatures and rotational momentum have shown to be overshadowed by ambient velocity fluctuations in the far wake [21]. Thus, ADs can create similar far wakes as rotating models, making them an appropriate substitution in the far wake, typically from three to four diameters downstream, both at low and high inflow turbulence [9, 13, 16, 17, 21]. Bossuyt et al. [12] found that the disks are acceptable when studying wake interactions at wind farm scale.

Despite the popularity of the simplified AD model, few experimental studies are available.

2.2 Numerical use of actuator disks

As mentioned, wind turbines are large, on the order of hundreds of meters, with a typical spacing within a wind farm of 5-10 diameters, and a thickness of the blade on the order of $1\ \mathrm{m}$. In order to resolve the full turbine geometry, ideally one would need to build a mesh with millimeter resolution around the blades inside a kilometer-scale computational box that the entire wind farm can fit within. As a consequence, simplifications are also used in Computational Fluid Dynamics (CFD). Many codes are based around the AD concept, leading to many researchers working with simulations based on ADs [10, 15, 16, 27, 28, 29, 30, 31]. Such modeling requires fewer grid cells and not as small dimensions, allowing larger time steps. However, this efficiency comes at the expense of resolving the fine details of the blade boundary layers. If the objective is to study the far wake, this trade off is reasonable and using ADs is more than acceptable. Work is being done in developing these models and comparing them to experimental results [10, 15], including an organized workshop to compare different state-of-the-art numerical models for the simulation of wind turbine wakes [32]. With further development, a relatively inexpensive tool for the assessment of flow fields and planning of wind farms would be at hand for the industry [14, 15].

2.3 Developing the actuator disk

One main issue related to ADs is that there is no standard for designing and making the disks today. Camp and Cal [33, 34] used a symmetric design in their research, with a solidity that decreases with radial direction. Bossuyt et al. [12] used a similar design, as well as Neunaber [9], who cut her disks from an aluminum plate. Aubrun et al. [21] used fine metal meshes with varying porosity at the center of the disc and at the outer edge. Later, Lignarolo et al. [16] used a layered fine metal mesh. Blackmore et al. [18] used a pattern of circular, equally-sized holes to maintain approximately uniform porosity across the radius. Theunissen et al. [22] used several different layouts, combining circular holes of different sizes as well as elongated bent fractures. Four years later, Theunissen et al. [23] once again used circular, equally-sized holes, comparing different topologies resulting in the same porosity. Sforza et al. [14] used perforated metal plates, while Pierella and

Sætran [19] used wooden grids and Myers et al. [35] used PVC plastic for their discs. In a series of tests conducted in 2019, both a metallic mesh with uniform porosity and a porous disc of plywood with radially non-uniform porosity were tested [13].

When doing research, it might vary which type of wind turbine one is trying to model, and thus the diameter, porosity and drag coefficient of the AD may vary. However, a standard design creating the desired wake would be practical in order to create uniformity and comparability between experiments, and to save time so that every researcher around the world does not need to start their research by developing their own disk from scratch.

Chapter 3

Method

In the following section the experimental setup will be explained. A short description of the RWTMs that were used will be given, followed by an explanation of the process of designing and creating the ADs. How the drag measurements in the wind tunnel were conducted and possible sources of uncertainty that occurred during the testing will also be highlighted. Finally, a summary of how the data was processed and how the calculations were conducted to find C_D will be given.

3.1 Experimental setup

In order to measure the drag on the RWTM and the ADs, a wind tunnel and a force plate was needed as part of the experimental setup. There was also the need to construct a test rig on which the models could be placed inside the wind tunnel, connecting them to the force plate.

3.1.1 Force plate, wind tunnel and associated equipment

The wind tunnel that was used is $1\ \mathrm{m}$ wide and $0.5\ \mathrm{m}$ tall. It has a maximum velocity of $35\ \mathrm{m\,s^{-1}}$. The wind velocity is changed by manually turning a wheel. The turbulence intensity is unknown, however it will be found when doing Particle Image Velocimetry (PIV) measurements in the continuation of this thesis. On the floor of the tunnel there is a small hole, making it possible to connect the item one is measuring forces on inside the tunnel to the load cell underneath the tunnel.

Underneath the wind tunnel is a AMTI BP400600HF 1000 force plate, able to measure the force and moment components along the x-, y- and z-axes. Here, x is in the downstream longitudinal direction, z is upwards and y completes the right-hand frame. The force plate has a maximum load of 2225 N in the x-direction. The A/D converter was configured to values corresponding to forces between -2.5 N and 2.5 N.

The drag measured by the load cell was sent as a voltage signal through an amplifier. Afterwards, it was sent through a low pass filter, with a cut-off frequency of 1000 Hz. The data was gathered and saved using LabView, and the signal was turned back into a force using the relationship between voltage and load provided by the manufacturer.

Inside the tunnel there is a sensor measuring the temperature, and a pitot tube measuring the pressure. The signal from the pitot tube was used to quantify the wind velocity.

A potential uncertainty related to the wind tunnel is the fact that the pitot tube is placed in the vertical center of the tunnel, about 4 m upstream of the WGTMs. Thus, the measured velocity was not necessarily the same as the velocity at the WGTMs, which were placed close to the floor of the tunnel. Due to the development of wall boundary layers, the velocity hitting the WGTMs was likely lower than the measured and registered velocity. The relationship between the centreline velocity and the hub height velocity will be established through PIV measurements at the start of the next term.

3.1.2 The rig

The test rig consists of a magnetic steel bar, 0.5 m long, stretching along the y-axis inside the wind tunnel, on top of an aluminum cylinder which connects the bar to an aluminum plate, that in turn can be attached to the load cell underneath the wind tunnel. Thus, the aluminum cylinder passed through the hole at the bottom of the wind tunnel, and then the rest of the hole was covered with tape. Careful consideration was taken when adding the tape, so that the aluminum cylinder did not touch anything, as that would affect the force measurements.

The bar was lifted about 1 cm above the floor of the wind tunnel. Initially, it was desired to have the steel bar be almost as long as the width of the wind tunnel, in order to produce a homogeneous blockage across the wind tunnel. Similarly, it was desired to have the hub of the turbines exactly in the middle of the tunnel to avoid the boundary layers. However, this was not structurally feasible. The hole in the bottom of the wind tunnel was limited in size, which meant that the steel bar could only be connected to the load cell underneath the tunnel through one aluminum cylinder with a small diameter of about 2 cm, making the support less robust. The length of the metal bar had to be shortened, and the bar had to be brought closer to the tunnel floor, in order to avoid bending and flapping at the ends.

3.2 Wind turbine models

The two-bladed rotating WGTMs are made at KTH Royal Institute of Technology in Stockholm, and can be seen in figure 3.1. They have a diameter of 45 mm, and a hub height of approximately 65 mm. Magnets are incorporated into the bottom of the models in order to mount them to a magnetic plate.

Figure 3.1: One of the rotating models.

3.3 The actuator disks

As mentioned, there is no standard way of designing ADs. In this project, the plan was to create ADs with multiple solidities, and a possible method would have been to create two ADs that were connected and could be rotated relative to each other in order to change the solidity. However, this seemed hard to achieve at such small scales. Pierella et al. [19] used PIV measurements, Pitot tube measurements and CFD simulations to study the flow behind two circular grids of equal diameter and porosity, one being a monoplane mesh and the other being a biplane mesh. The results showed that the biplane disk produced a lower drag than the monoplane disk, and that the two induced different wakes. The monoplane disk incuded an axisymmetric wake, while the biplane disk induced a non-axisymmetric flow dominated by the presence of trailing vortices. Thus, these two cases are not directly comparable, and since the goal of this project was to develop an AD that does not induce a rotational element onto the flow, the monoplane disk was chosen.

3.3.1 Computer-aided design and 3D printing

The ADs, as well as their towers, were designed using SolidWorks. Cura was used to turn the designs into readable code for the 3D printers, and the parts were then printed using a printer of the type Ultimaker 2+. The material used was PLA.

A significant limitation occurred during the design process. The 3D printers available could not print thinner than $0.4\ \mathrm{mm}$, meaning that each line in the disks had to be at least $0.4\ \mathrm{mm}$. However, printing lines of $0.4\ \mathrm{mm}$ proved troublesome, and it was decided that all lines should be equal to or thicker than $0.5\ \mathrm{mm}$. This is significant given that the disks

Figure 3.2: The 3D printed tower.

are in themselves of such small dimensions. So there turned out to be a limit to how porous the disks could be made.

3.3.2 Design of the tower

The tower was designed to have the exact same dimensions as the given RWTM's tower. Most importantly, it had a hub height of 65 mm. Underneath the base a hole was made that could fit a cylindrical neodymium magnet with a diameter of 10 mm, a height of 2.5 mm and a holding strength of 0.9 kg. The ADs were made to be interchangeable, and the end of the tower where the ADs would be connected was made slightly thinner in order to fit into the designated holes in the ADs. Three towers were printed, and one of them can be seen in figure 3.2.

3.3.3 Actuator disk design

The ADs were designed with a diameter of 45 mm, to match the RWTMs. In an effort to have the same volume of the AD as the swept volume of the blades, the blade is pointed straight down, and its projection on the zx-plane is studied. The thickest part of the projected blade is measured to be 5 mm, whilst the thinnest part has approximately zero width. The thickest part is at the blade tip while the thinnest part is at the hub. Approximating the area of the blades when seen from the side as a triangle with height equal to the radius of the blade and base length equal to 5 mm gives an estimate of the swept area, which is rotated around the hub to give the swept volume. In order to approximate the area with an AD of constant width, the width should be half the size of the thickest part of the blades,

i.e. 2.5 mm. This gives approximately the same volume of the AD as the swept volume of the blades.

Two different designs of ADs were tested. The first has numerous equally-sized holes spread symmetrically around the center point of the disk, as seen in figure 3.3a and 3.4a. It is quite similar to the design of Blackmore et al. [18]. The design is also meant to be comparable to those AD designs that consist of a thin metal grid, similar to a grid turbulence generator, as used by Aubrun et al. and Lignarolo et al. [16, 21]. The disks with this design will be called Uniform Holes Disk (UHD) going forth. The second design is also symmetric around the center point, but this one has rectangular holes that vary in size with radial distance, increasing in size as the radial coordinate increases, as seen in figure 3.3b and 3.4b. Thus, the solidity decreases with radial coordinate, matching the characteristics of an actual wind turbine. This design was used by Camp and Cal [33, 34] and by Neunaber [9]. This design will be called Non-Uniform Disk (NUD).

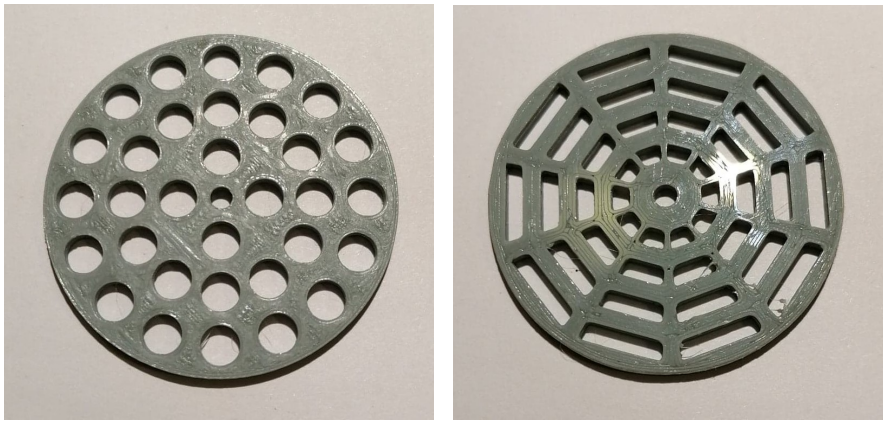

(a) The UHD design. **(b)** The NUD design.

Figure 3.3: Actuator disks with a solidity of 60%.

For each of these configurations, two solidities were created as an initial trial. The chosen solidities were 60% and 40%. A solid disk was also made as a reference case. Three disks of each design and solidity were printed.

Based on the resulting drag profiles from the initial round of testing, two sets of ADs with a solidity of 35% were designed and printed, which can be seen in figure 3.5a and 3.5b. The first was made based on the UHD design. Due to the mentioned limitations regarding the printing thickness, providing a solidity less than 39% with this design proved problematic. Hence the design was slightly changed, allowing for the holes to also cover the edges of the ADs. It was kept in mind that this results in a different disk circumference, and that this might result in a drag force that is not directly comparable to the drag of the previously tested disks with the UHD design. The second disk was made using the NUD design.

Each disk was, as mentioned, made with a small hole in the center, used to connect the disks to the tower. When connecting the two, this hole was filled in by the end of the tower,

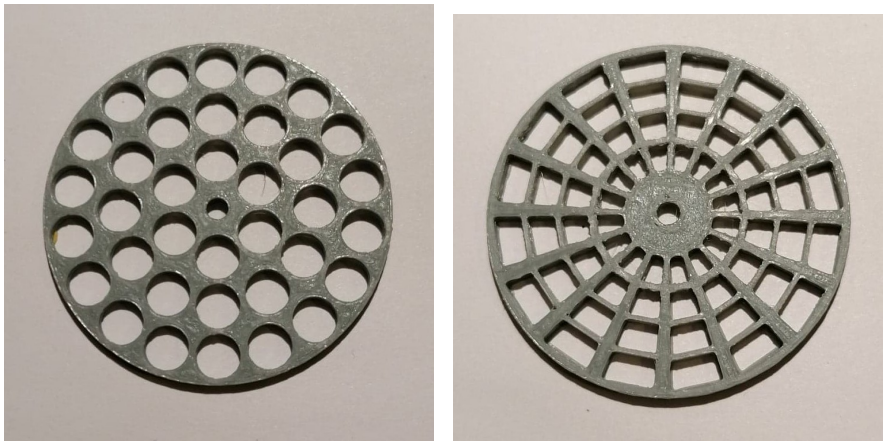

(a) The UHD design. **(b)** The NUD design.

Figure 3.4: Actuator disks with a solidity of 40%.

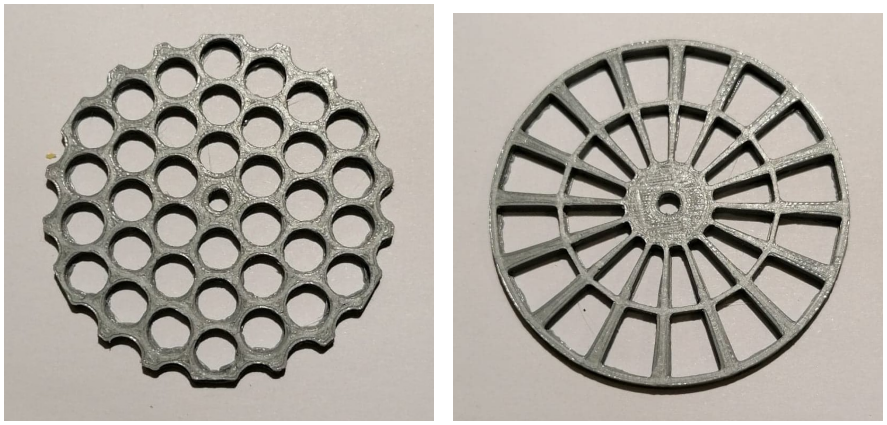

(a) The UHD design. **(b)** The NUD design.

Figure 3.5: Actuator disks with a solidity of 35%.

and so it did not affect the solidity of the disk. This design resulted in a larger solidity in the center of the disks, which can be argued to represent the nacelle of a wind turbine. A disk connected to a tower can be seen in figure 3.6.

3.4 Testing

Given that the size of the WGTMs was quite small, the models were tested in the wind tunnel three at a time, to ensure that the drag would be of an order that the instruments were able to measure and of an order where slight changes in the design and the resulting

Figure 3.6: The 3D printed tower connected to the 3D printed NUD with 35% solidity.

slight changes in drag would be noticeable. The WGTMs were placed along the steel bar such that one model was in the center of the tunnel, and the other two were placed symmetrically on each side, with a distance of 4D between them.

Even though the RWTM were magnetic, it proved problematic to make them stay in the same position, with the turbine perpendicular to the incoming flow direction, especially as the wind velocity increased. Thus, the rotating models were connected to the steel bar using small pieces of tape. The 3D printed towers were able to stay in the right position on the bar by themselves. Still, they were taped to the base like the RWTMs, to make sure the cases were comparable.

As the drag was the only force of interest in this work, only the force in the x-direction was measured. The force was measured for five different wind velocities; 5 $\mathrm{m\,s^{-1}}$, 7.5 $\mathrm{m\,s^{-1}}$, 10 $\mathrm{m\,s^{-1}}$, 12.5 $\mathrm{m\,s^{-1}}$ and 15 $\mathrm{m\,s^{-1}}$. This corresponds to Reynolds numbers $Re = \frac{\rho U D}{\mu} \approx 1.5 * 10^4$, $\approx 2.3 * 10^4$, $\approx 3.0 * 10^4$, $\approx 3.7 * 10^4$ and $\approx 4.5 * 10^4$, respectively. When calculating Reynolds number, the characteristic length used is the diameter of the ADs, 0.045 m. Since the velocity was changed by manually turning a wheel, a small difference in the velocities occurred between the different measurement sets.

The force plate drifted over time, as is often the case with force measuring equipment. To take this into consideration when measuring the forces, zero measurements were conducted before and after every measurement. A 20 s tare measurement was first conducted. The wind tunnel was then turned on, with the velocity initially set to about 1 $\mathrm{m\,s^{-1}}$, and then turned up to the desired value. A measurement lasting 60 s was then conducted. The velocity was once again reduced to about 1 $\mathrm{m\,s^{-1}}$, and the wind tunnel was shut off. After

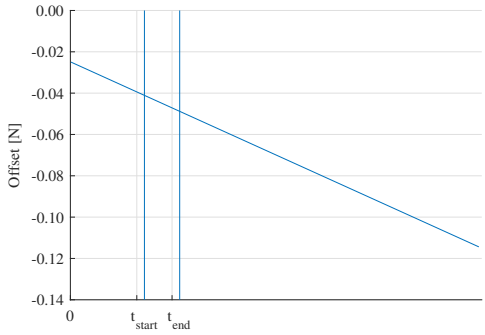

Figure 3.7: The approximated drift between the two zero measurements. t_{start} indicates where the 60 s measurement started, and t_{end} indicates where the measurement ended.

the wind tunnel had quiet down and there was close to no moving air inside, another 20 s tare measurement was conducted. The wind tunnel needed about 10 min before one could be sure that the air inside was still, meaning that the measurements were quite time consuming. When measuring, a sampling rate of 1000 Hz was used.

Besides measuring the drag on the RWTMs and on all the different sets of ADs, a set of measurements was also acquired measuring the drag on only three towers, without any disks connected to them. Thus, the drag of the base and the towers was quantified.

3.5 Calculations

For each WGTM at each wind velocity, the data collected from the wind tunnel consisted of a time series of voltages corresponding to the measured drag force and the measured wind velocity, as well as the points in time when the first zero measurement and the second zero measurement were conducted and when the 60 s drag measurement started. The data was processed using Matlab.

The force plate was assumed to drift linearly. Thus, using the two zero measurement values, a linear function approximating the drift was created. The part of this linear function corresponding to the 60 s where the force measurement was conducted, was extracted, as seen in figure 3.7. For each measured force in the time series, the corresponding drift was subtracted. Afterwards, the average drag force over the time series was calculated, as well as the variance and standard deviation.

It turned out that not adjusting the measurements to account for the drift of the force plate only resulted in minimal differences in the drag coefficient. However, the drift was accounted for, to make sure the measurements were as accurate as possible.

In the same manner, the drift was subtracted and the average drag force was calculated for the measurements that were conducted using only the bar and the towers, for each of the different wind velocities. These average drag forces were then subtracted from the averages drag forces calculated earlier for all the different WGTMs, so that what remains

is only the drag on the disks or the turbine blades, excluding the towers and the base.

Finally, this calculated drag was divided by three, so as to only consider the drag on one disk or one set of rotating blades. This force was further used in calculating the drag coefficient, using equation 2.1, together with the total swiping area of the rotating turbine model, being πr^2.

Another value collected as part of the measurement data was the average temperature during the 60 s of measuring. This was used to decide on the appropriate value for the air density, ρ, and air dynamic viscosity, μ, when calculating the drag coefficient and the Reynolds number. However, the temperature only varied between about 20°C and 23°C.

Chapter 4

Results & Discussion

During the measurement phase, it turned out that several measurement sets needed to be conducted for the rotating models, due to several deviations in the data. In this section, the measurement data and the process of treating it will be presented, together with the final average drag coefficient of the rotating models. After this, the drag and drag coefficient of all the different ADs will be presented and compared to the average results for the rotating models.

4.1 Rotating models

The first measurement set conducted using three RWTMs resulted in a drag coefficient that seemed relatively independent of Reynolds number for four of the measured Reynolds numbers, but with a noticeable deviation at $Re \approx 1.5 * 10^4$. To investigate whether this deviation was due to a measurement error, a second measurement set was conducted, this time using three new RWTMs. This second measurement gave more of an expected result at $Re \approx 1.5 * 10^4$, however showed a deviation at $Re \approx 4.5 * 10^4$. Due to continuous deviations, however differing in size and appearing at different Reynolds numbers, six measurements were eventually conducted. They were all done with different sets of RWTMs, except for measurement set three and four, which were done using the same set of models. The resulting drag coefficients can be seen as a function of Re in figure 4.1.

As can be seen, there is some variation between the different measurements. The drag coefficients resulting from the third and the fourth measurement set, conducted using the same models, are quite similar at $Re \approx 1.5 * 10^4$, $Re \approx 2.3 * 10^4$ and $Re \approx 3.7 * 10^4$, and at $Re \approx 4.5 * 10^4$ they completely overlap. This seems to show that the measurement is to some degree repeatable, and that one of the reasons for the varying results is simply that there are small differences between the RWTMs. These differences can for example be related to the friction between the rotating blades and the hub that they rotate around. In addition, the blades stay onto the hub due to a small piece of transparent plastic, that

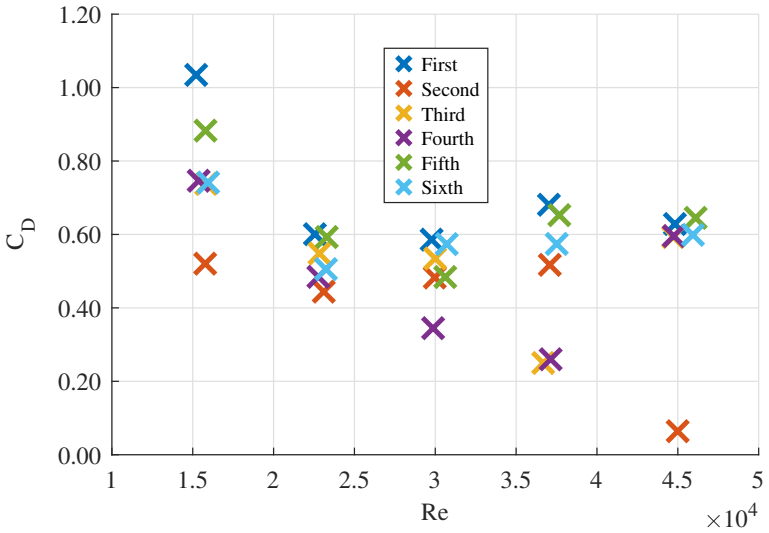

Figure 4.1: The drag coefficient for the rotating models, obtained through six rounds of measurements.

differs in size between the models. If it is too big, it might fasten the blades too tightly, causing added friction. If it is too small, the blades might be too loose, and they may start to oscillate. These types of differences were evident during the measurement phase, as several times the measurements had to be stopped midway due to one of the turbines suddenly not rotating anymore, and once because the rotating blades fell of the model.

However, even between the third and fourth measurement set, there is a noticeable difference at $Re \approx 3 * 10^4$, showing that differences between the RWTMs is not the only cause for the varying results. Other possible causes of this variation may be related to fluctuations in the applied wind velocity and to noise in the transducer and the electrical equipment used. Human error is also an important factor, as the models were placed in the wind tunnel by hand, and the turbine blades were not necessarily always exactly perpendicular to the incoming flow direction.

To investigate the results further, the drag resulting from the different measurements were plotted as a function of Reynolds number, as seen in figure 4.2.

The drag at $Re \approx 4.5 * 10^4$ is significantly lower than the drag at $Re \approx 3.7 * 10^4$ for the second measurement set. The same is the case for the third measurement set, where the drag at $Re \approx 3.7 * 10^4$ is significantly lower than the drag at $Re \approx 3 * 10^4$. For the drag to decrease with increasing Re is not physical within this range of Reynolds numbers, and thus these two measurements are assumed to be outliers.

The measurements at $Re \approx 3.7 * 10^4$ were studied further. By visual inspection there seems to be a cluster at around 0.09 N, while the fourth measurement seems to be outside this cluster. This is confirmed by the fact that the distance between the fourth measurement and the mean of the cluster is over four times the standard deviation of the cluster. It is

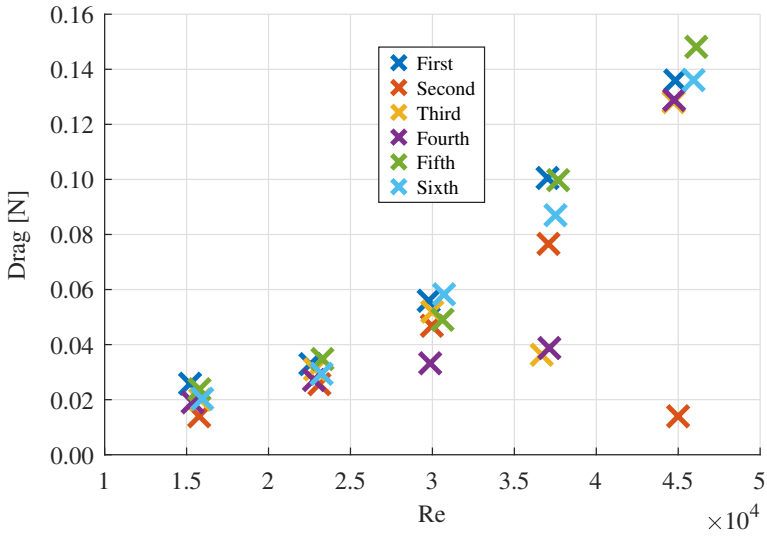

Figure 4.2: The measured drag for the rotating models, obtained through six rounds of measurements.

worth noting that this outlier is close to the already discarded drag measurement from the third measurement set. These two measurement sets used the same rotating models and both showed a considerable amount of noise on the signal for Reynolds numbers around $3.2 * 10^4 - 3.9 * 10^4$, which was not observed for the other measurement sets. Thus, these specific rotating models might be the reason for the repeated deviation at $Re \approx 3.7 * 10^4$.

A similar study was conducted for $Re \approx 3 * 10^4$. By visual inspection, five of the measurements seem to coincide at around 0.05 N, while the fourth measurement seems to be outside this cluster. Once again, this is confirmed by the fact that the distance between the fourth measurement and the mean of the cluster is over four times the standard deviation of the cluster.

In total, four measured drags have been discarded, and the four associated drag coefficients were removed. In order to achieve a representative value for the drag coefficient of the RWTMs, the average of the remaining drag coefficients was taken at each Reynolds number. This resulted in the drag coefficients seen in figure 4.3. It is assumed that the drag measurements have a Gaussian distribution about some mean value, and that this calculated average based on six measurements is representative for the average one would have gotten if all the rotating models had been tested and all the tests had been conducted multiple times. It should be noted that this uncertainty related to the rotating models, causing the need for taking the average over several measurements, supports the claim that there is a need for alternative ways of modelling wind turbines.

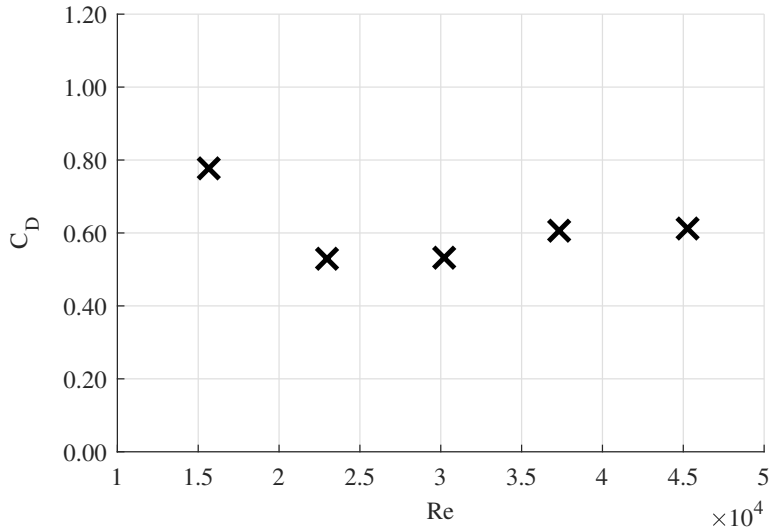

Figure 4.3: The average drag coefficient for the rotating models at each Reynolds number, based on the six conducted measurements, after removing the assumed errors and outliers.

4.2 Drag on the actuator disks

The measured drag and the calculated drag coefficients related to the produced ADs have been studied. The solid disk, used as a reference case, produced the drag seen in figure 4.4a and the drag coefficient seen in figure 4.4b. There seems to be a deviation of the drag coefficient at $Re \approx 3 * 10^4$, however, due to limited time and the fact that the solid disk was far from comparable to the rotating models, the measurements were not redone. Further, the drag and the drag coefficient for the two types of disks with 60% solidity can be seen in figure 4.5a and 4.5b, respectively.

The drag for the disks with 40% and 35% solidity were plotted in figure 4.6, and the

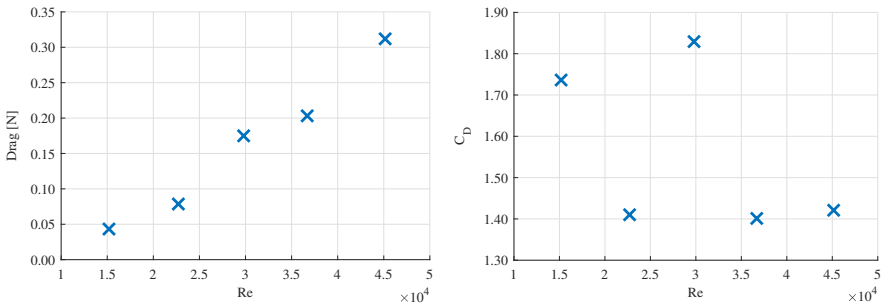

(a) The drag.

(b) The drag coefficient.

Figure 4.4: Using the solid disk.

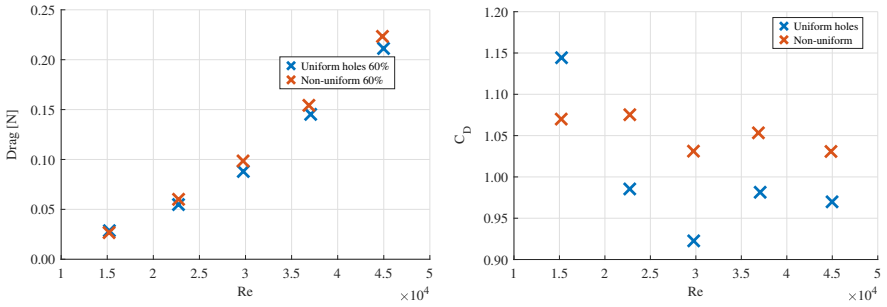

(a) The drag. **(b)** The drag coefficient.

Figure 4.5: Using the disks with 60% solidity.

drag coefficient for the same disks were plotted in figure 4.7. As these disks produced a drag fairly close to the average drag of the RWTMs, the average drag and drag coefficient representing the rotating models is also included in the plots, to ease the comparison.

Some general trends can be observed from these graphs. For all the AD and RWTM measurements, the drag is seen to increase with increasing Re, as one would expect. Another trend that can readily be seen, is that the drag coefficient increases with increasing solidity. This coincides with what has been found in the literature. Lignarolo et al. [16] presented a comparison between different drag coefficients as a function of solidity, based on the results presented in six different papers. Compared, the ADs used in this current study results in a slightly higher drag coefficient for all the solidities. This can be caused by differences in inflow conditions, such as inflow turbulence, or be due to the models being placed in the boundary layer in this study, in contrast to most cases in literature where the hub is in the free stream flow. However, Lignarolo et al. also concludes that the drag coefficient seems to be approximately linearly decreasing with decreasing solidity, which is the case with the current measurements as well.

For all the different ADs and for the RWTMs, the drag coefficient corresponding to $Re \approx 1.5 * 10^4$ is significantly higher than for the other Reynolds numbers, while the drag coefficient related to the other four Reynolds numbers generally seem to concentrate around some mean value. This deviation at $Re \approx 1.5 * 10^4$ might be caused by measurement noise. When studying the standard deviation for each 60 s measurement, the standard deviation is always between 0.011 and 0.015, independent of which disk is being studied, showing that this is probably the size of the measurement noise related to the transducer and electrical equipment. The drag force at such a low velocity will be quite small, and it seems that the measurement noise might be larger than the actual drag and interfering with the measurements. Additionally, it should be pointed out that the drag coefficient at low velocities is much more sensitive to small changes in drag compared to at higher velocities, resulting from equation 2.1. However, this result will not have any significant impact on the future work, as the future work will focus around Reynolds numbers higher than $Re \approx 1.5 * 10^4$.

Looking at figure 4.7, the NUD with 35% solidity and the UHD with 35% solidity seem

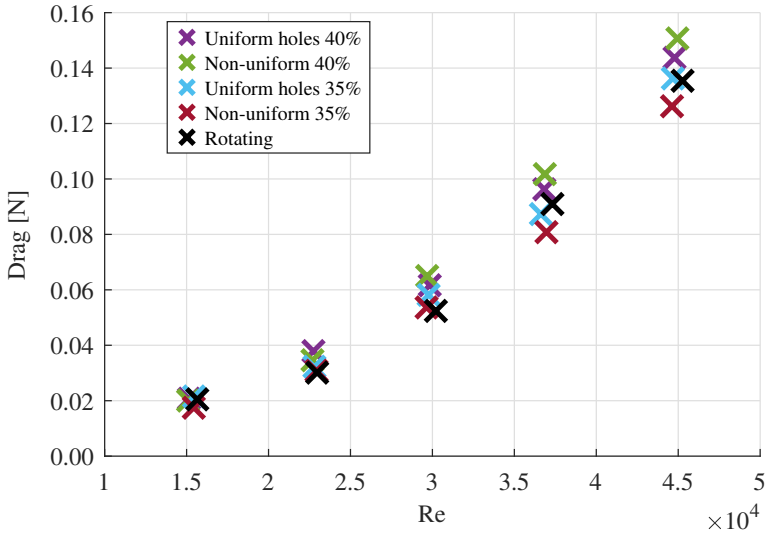

Figure 4.6: The drag for the disks with 40% and 35% solidity, compared to the average drag coefficient of the rotating disks.

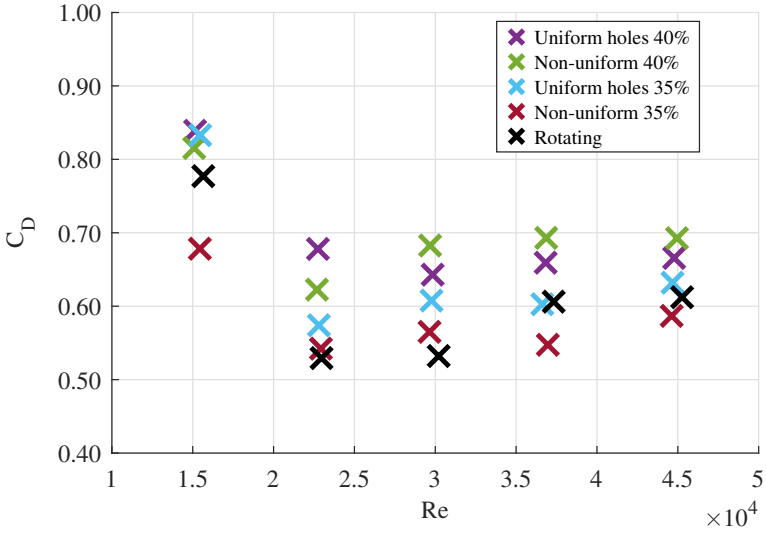

Figure 4.7: The drag coefficient for the disks with 40% and 35% solidity, compared to the average drag coefficient of the rotating disks.

Disk type	Average C_D	C_D standard deviation
Rotating average	0.570	0.082
Uniform holes, 40%	0.662	0.053
Non-uniform, 40%	0.673	0.057
Uniform holes, 35%	0.604	0.051
Non-uniform, 35%	0.560	0.051

Table 4.1: Average C_D for the rotating model and the disks with 35% solidity.

to best match the drag of the rotating model. To study this further, the average drag coefficient over the four Reynolds numbers where the measurements already seem to gather around some mean, is calculated, and presented in table 4.1. The standard deviation is also included, as well as the average C_D and the standard deviation for the 40% ADs. If one assumes that the C_D corresponding to the rotating model is correct, and that the ADs have a Gaussian distribution, it can be seen that the standard deviation of both disks with 35% solidity covers the rotating C_D value, while neither of the 40% solidity disks do. Thus, it is concluded that the disks with 35% solidity is the best match, and based on the averages it seems that the NUD with 35% solidity is the closest match, while the UHD with 35% solidity is the second closest.

An additional remark that can be made is that there does not seem to be a clear trend regarding the drag produced when using the NUD design compared to the drag produced when using the UHD design, in terms of one design consistently producing a larger or a smaller drag than the other.

Chapter 5

Future work

As concluded by Theunissen et al. [22], in order to create an AD matching a RWTM, the wake must be similar. Matching the drag coefficient is only the first step in this process.

Going forth, the rotating models and the two ADs with the closest matching drag coefficient will be studied using PIV. Both the flow in front of the models and the wake behind the models will be studied. This method can be used to examine the velocity deficit and the turbulence intensity in the wake. It is also desireable to integrate the wake in order to find and compare the axial induction factor. The problem with using monoplane ADs is the lack of a way to add a rotational momentum to the flow, and the effect of this will be studied.

Further, the plan is to acquire 100-150 RWTMs, and set them up as a wind farm in a larger wind tunnel. Equally many ADs will be made, using the design that most closely matches the drag and the wake, and the ADs will also be set up as to simulate an entire wind farm. This will be done in order to study the similarities and differences between the models when used for wind farm modelling, and to some extent determine the suitability of using ADs when modelling large wind farms.

Chapter 6

Conclusion

In this project report, an actuator disk that has a similar drag to a two-bladed rotating wind turbine model is found. The actuator disks were created using computer-aided design. Two different designs were tested, one with uniform holes inspired by the work of Aubrun et al. [21], and one non-uniform design based on the disks used by Camp and Cal [33]. The disks were made with three different solidities, 60%, 40% and 35%. A solid disk was made as a reference case. All the disks had a hole in the center, used to connect them to the towers, thus making the disks interchangeable. The disks, as well as the towers, were 3D printed using PLA.

Experiments were conducted using three models at the same time, to make sure the drag would be of an order where slight changes in solidity and the resulting slight changes in the drag would be noticeable by the force plate being used. Measurements were done at five different Reynolds numbers, all of the order 10^4. Initial tests showed that the force plate drifted over time. To solve this, zero measurements were conducted before and after each measurement. A linear drift was assumed, and for each measurement, the corresponding drift was subtracted. Not adjusting the measurements to account for the drift of the force plate only resulted in minimal differences in the drag coefficient, but the drift was still accounted for, to achieve more accurate results. Measurements were also conducted using only the towers and the bar that the models were placed on inside the tunnel, so that this drag could be subtracted from the previous drag measurements, leaving only the drag on the disks and on the rotating blades.

When conducting the measurements of the rotating models, some of the resulting drag coefficients deviated from the rest, however these deviations differed in size and appeared at different Reynolds numbers. Thus, six measurement sets were conducted, all using different sets of rotating models, except for two of them which used the same models. The reasons behind the deviations were concluded to be variations between the rotating models, noise in the transducer, and human error. It was solved by discarding those measurements regarded as outliers, and taking the average of the remaining drag coefficients at each

Reynolds number. This uncertainty related to the rotating models supports the claim that there is a need for alternative ways of modelling wind turbines.

The drag and drag coefficients deriving from all the different actuator disks were then studied. Some general trends showed that the drag increases with increasing Re, and that the drag coefficient increases with increasing solidity, as supported by literature [16]. Additionally, the drag coefficient seems to be Reynolds number independent for four of the Reynolds numbers, but the drag coefficient at $Re \approx 1.5 * 10^4$ deviates from the others, most likely due to the impact of noise on such a small drag and the increased sensitivity to drag deviations at such a low velocity. Based on the average drag coefficient calculated across the different Reynolds numbers, excluding $Re \approx 1.5 * 10^4$, the non-uniform disk with 35% solidity seems to best match the rotating model, while the 35% solidity disk with uniform holes is the second closest match. Assuming a Gaussian distribution of the drag coefficients, both of the disks with 35% solidity had the rotating models drag coefficient within its standard deviation, and vise versa, showing that it is reasonable to use these actuator disks to mimic the rotating model.

In future work, the wakes of these two models will be studied using Particle Image Velocimetry, and compared to the wake of the rotating model, investigating factors such as velocity deficit, turbulence intensity and rotation of the flow. The models will also be used to simulate a wind farm, and similarities and differences between the resulting flow fields will be studied.

Bibliography

[1] J. V. C. Nye. Standards of living and modern economic growth. https://www.econlib.org/library/Enc/StandardsofLivingandModernEconomicGrowth.html, 2008. [Online; accessed 12-December-2019].

[2] K. Haanaes. Why all businesses should embrace sustainability. https://www.imd.org/research-knowledge/articles/why-all-businesses-should-embrace-sustainability/, 2016. [Online; accessed 12-December-2019].

[3] P. Veers, K. Dykes, E. Lantz, S. Barth, C. Bottasso, O. Carlson, A. Clifton, J. Green, P. Green, H. Holttinen, D. Laird, V. Lehtomäki, J. Lundquist, J. Manwell, M. Marquis, C. Meneveau, P. Moriarty, X. Munduate, M. Muskulus, and R. Wiser. Grand challenges in the science of wind energy. *Science*, page eaau2027, 10 2019.

[4] WindEurope. History of Europe's wind industry. https://windeurope.org/about-wind/history/, 2019. [Online; accessed 12-December-2019].

[5] International Renewable Energy Agency. Renewable energy now accounts for a third of global power capasity. https://www.irena.org/newsroom/pressreleases/2019/Apr/Renewable-Energy-Now-Accounts-for-a-Third-of-Global-Power-Capacity, 2019. [Online; accessed 12-December-2019].

[6] Siemens. The socioeconomic impacts of wind energy in the context of the energy transition. https://www.siemensgamesa.com/explore/journal/socioeconomic-report-wind-energy-2019, 2019. [Online; accessed 12-December-2019].

[7] J. Meyers and C. Meneveau. Optimal turbine spacing in fully developed wind farm boundary layers. *Wind Energy*, 15:305 – 317, 03 2012.

[8] R. Stevens and C. Meneveau. Flow structure and turbulence in wind farms. *Annual Review of Fluid Mechanics*, 49, 01 2017.

[9] I. Neunaber. *Stochastic investigation of the evolutoon of small-scale turbulence in the wake of a wind turbine exposed to diffeent inflow conditions*. PhD thesis, Carl von Ossietzky Universitat Oldenburg, 11 2018.

[10] L. Martínez-Tossas, M. Churchfield, and S. Leonardi. Large eddy simulations of the flow past wind turbines: actuator line and disk modeling: Les of the flow past wind turbines: actuator line and disk modeling. *Wind Energy*, 18, 04 2014.

[11] F. Porté-Agel, M. Bastankhah, and S. Shamsoddin. Wind-turbine and wind-farm flows: A review. *Boundary-Layer Meteorology*, 09 2019.

[12] J. Bossuyt, M. Howland, C. Meneveau, and J. Meyers. Measurement of unsteady loading and power output variability in a micro wind farm model in a wind tunnel. *Experiments in Fluids*, 58, 12 2016.

[13] S. Aubrun, M. Bastankhah, R.B. Cal, B. Conan, R.J. Hearst, D. Hoek, M. Hölling, M. Huang, C. Hur, B. Karlsen, I. Neunaber, M. Obligado, J. Peinke, M. Percin, L. Saetran, P. Schito, B. Schliffke, D. Sims-Williams, O. Uzol, M.K. Vinnes, and A. Zasso. Round-robin tests of porous disc models. *Journal of Physics: Conference Series*, 1256:012004, jul 2019.

[14] P. Sforza, P. Sheerin, and M. Smorto. Three-dimensional wakes of simulated wind turbines. *Aiaa Journal - AIAA J*, 19:1101–1107, 09 1981.

[15] M.E. Harrison, W. Batten, L. Myers, and A. Bahaj. Comparison between cfd simulations and experiments for predicting the far wake of horizontal axis tidal turbines. *Renewable Power Generation, IET*, 4:613 – 627, 12 2010.

[16] L. Lignarolo, D. Ragni, C. Ferreira, and G. van Bussel. Experimental comparison of a wind-turbine and of an actuator-disc near wake. *Journal of Renewable and Sustainable Energy*, 8:023301, 03 2016.

[17] L. Lignarolo, D. Ragni, C. Ferreira, and G. van Bussel. Kinetic energy entrainment in wind turbine and actuator disc wakes: An experimental analysis. *Journal of Physics: Conference Series*, 524:012163, 06 2014.

[18] T. Blackmore, W. Batten, G. Muller, and A. Bahaj. Influence of turbulence on the drag of solid discs and turbine simulators in a water current. *Experiments in Fluids*, 55, 12 2013.

[19] Fabio Pierella and Lars Sætran. Effect of initial conditions on flow past grids of finite extension. *17th Australasian Fluid Mechanics Conference 2010*, 01 2010.

[20] S. Cannon, F. Champagne, and A. Glezer. Observations of large-scale structures in wakes behind axisymmetric bodies. *Experiments in Fluids*, 14:447–450, 05 1993.

[21] S. Aubrun, S. Loyer, P. Hancock, and P. Hayden. Wind turbine wake properties: Comparison between a non-rotating simplified wind turbine model and a rotating model. *Journal of Wind Engineering and Industrial Aerodynamics*, 120:1–8, 09 2013.

[22] R. Theunissen, P. Housley, C. Allen, and C. Carey. Experimental verification of computational predictions in power generation variation with layout of offshore wind farms. *Wind Energy*, 18, 07 2014.

[23] R. Theunissen and R. Worboys. Near-wake observations behind azimuthally perforated disks with varying hole layout and porosity in smooth airstreams at high reynolds numbers. *Journal of Fluids Engineering*, 141, 09 2018.

[24] W. Zhang, C. Markfort, and F. Porté-Agel. Near-wake flow structure downwind of a wind turbine in a turbulent boundary layer. *Experiments in Fluids*, 52, 05 2012.

[25] R. J. Barthelmie and L. E. Jensen. Evaluation of wind farm efficiency and wind turbine wakes at the nysted offshore wind farm. *Wind Energy*, 13, 04 2010.

[26] R. J. Barthelmie and L. E. Jensen. Evaluation of wind farm efficiency and wind turbine wakes at the nysted offshore wind farm. *Wind Energy*, 13, 04 2010.

[27] Y.T. Wu and F. Porté-Agel. Large-eddy simulation of wind-turbine wakes: Evaluation of turbine parametrisations. *Boundary-Layer Meteorology*, 138, 03 2011.

[28] Y.T. Wu and F. Porté-Agel. Atmospheric turbulence effects on wind-turbine wakes: An les study. *Energies*, 5:5340–5362, 12 2012.

[29] N. Simisiroglou, S.P. Breton, and S. Ivanell. Validation of the actuator disc approach using small-scale model wind turbines. *Wind Energy Science*, 2:587–601, 11 2017.

[30] R. Stevens and C. Meneveau. Temporal structure of aggregate power fluctuations in large-eddy simulations of extended wind-farms. *Journal of Renewable and Sustainable Energy*, 6, 12 2014.

[31] R. Stevens, D. Gayme, and C. Meneveau. Large eddy simulation studies of the effects of alignment and wind farm length. *Journal of Renewable and Sustainable Energy*, J. of Renewable and Sustainable Energy 6, 023105 (2014), 05 2014.

[32] L. Lignarolo, D. Mehta, R. Stevens, A. Yilmaz, G. Kuik, S. Andersen, C. Meneveau, C. Ferreira, D. Ragni, J. Meyers, G. van Bussel, and J. Holierhoek. Validation of four les and a vortex model against stereo-piv measurements in the near wake of an actuator disc and a wind turbine. *Renewable Energy*, 94:510–523, 08 2016.

[33] E. Camp and R.B. Cal. Mean kinetic energy transport and event classification in a model wind turbine array versus an array of porous disks: Energy budget and octant analysis. *Physical Review Fluids*, 1:044404, 08 2016.

[34] E. Camp and R.B. Cal. Low-dimensional representations and anisotropy of model rotor versus porous disk wind turbine arrays. *Physical Review Fluids*, 4, 02 2019.

[35] L. Myers and A. Bahaj. Experimental analysis of the flow field around horizontal axis tidal turbines by use of scale mesh disk rotor simulators. *Ocean Engineering*, 37:218–227, 02 2010.